UC
UNIVERSIDAD DE CANTABRIA

Facultad de Ciencias

SIMULACIÓN RÁPIDA DE TRANSITORIOS DE CORRIENTE EN DETECTORES DE SILICIO IRRADIADOS
(Fast simulation of transient currents in irradiated silicon detectors)

Trabajo de Fin de Grado
para acceder al

GRADO EN FÍSICA

Autor: Álvaro Díez González-Pardo

Director: Marcos Fernández García

Co-Director: Iván Vila Álvarez

9 - Enero - 2017

A mi madre y mi padre que han soportado con una sonrisa innumerables charlas sobre física y que aunque no entiendan inglés se alegran de ver este trabajo más que nadie

Contents

0.1 Keywords

Software de simulación, Detectores de Silicio, Detectores irradiados, Física de altas energías

Simulation software, Particle detectors, Silicon detectors, Irradiated detectors, High energy physics

Acknowledgements

UNIVERSIDAD DE CANTABRIA

Abstract

Facultad de Ciencias

Bachelor of Physics

Developing a fast simulator for irradiated silicon detectors

by Alvaro Diez Gonzalez-Pardo

El software de simulación TRACS ha sido mejorado para incluir los efectos de la radiación en los detectores de silicio. El daño por radiación ha sido parametrizado en términos del perfil de distribución espacial de la carga (N_{eff}) y la probabilidad de atrapamiento de los portadores (a través del tiempo de atrapamiento τ). Dentro del software es posible definir el N_{eff} utilizando una de las tres diferentes parametrizaciones. Dependiendo de la parametrización el usuario deberá definir el N_{eff} ajustando entre 2 a 6 parámetros libres. La funcionalidad de TRACS también ha sido ampliada pudiendo ser utilizado como un libreria dentro de software externo. Las simulaciones de detectores de silicio irradiados han sido comparadas con medidas experimentales y muestra acuerdo dentro del error estimado para las simulaciones de TRACS.

Existing simulation software TRACS[1] has been upgraded to account for radiation effects in silicon detectors. Radiation damage has been parametrised in terms of the space charge distribution (N_{eff}) profile and the probability of carrier trapping (through the trapping time τ). It is possible to define the N_{eff} profile using three different parametrisations. Depending on the parametrisation, the user needs to adjust between 2 and 6 parameters to properly define the N_{eff} profile. TRACS has also been extended to be used by external software as a library. The simulations of irradiated silicon detectors have been compared to measurements and show agreement withing the estimated error for TRACS simulations.

Chapter 1

Introduction

There are many kinds of particle detectors in High Energy Physics ranging from the first Bubble and Cloud Chambers up to the latest High Voltage CMOS (Complementary Metal Oxide) solid state detectors. Their design varies depending on many parameters: application, magnetic field, operational temperature, active medium, measurement rate, layout, radiation damage they need to withstand... making it possible to optimise detectors for specific needs. During the past decades, silicon has become the technology of choice for tracking detectors, as it tends to offer an excellent compromise between energy, space and time resolution at a fairly moderate price. Another advantage of silicon detectors is the existing R&D for other applications, and the possibility to go on commercial technologies.

The scope of this work is the modelling of the performance of silicon detectors exposed to high fluence of particles, such as those existing in particle accelerators, like the Large Hadron Collider (LHC) at CERN[1] and future ones, like its High Luminosity upgrade(HL-LHC) . There, the innermost tracking detectors will have to withstand particle fluences up to 10^{16} n_{eq}/cm^2 during 10 years of operational lifetime. The amount of collected charge will decrease over this period due to trapping of charge carriers in radiation induced traps. The detectors will have to be designed such that the charge loss is above an electronics threshold of ≈ 6000 e^-, which is the minimum the electronics can resolve.

Understanding the effects of radiation in Si is a crucial task. These detectors have to operate for a period of 10 years without being replaced. In this project, a model of radiation damage in silicon has been implemented into an already existent simulation software called TRACS[1].

---

[1]European Organization for Nuclear Research, the acronym is derived from its former name in french: Conseil Européen pour la Recherche Nucléaire

In Chapters 2 and 3 we will introduce some background information on how silicon detectors work and how radiation affects their internal structure and performance. Chapter 4 will describe an experimental technique used in this work to characterise silicon detectors. This data will serve as an input to crosscheck the results of the simulation. In chapter 5 the inner workings of the software and the actual implementation of radiation damage is presented. Finally, chapter 6 will show a comparison between simulation and experimental data to prove the validity of the simulations.

Chapter 2

Silicon detectors basics

In general, a solid state detector consists of an enclosed volume, filled with a material in which free charge carriers can be generated by an incident particle. This sensing volume is generally connected to a power supply that provides a potential difference between two points inside the volume. The potential difference induces the movement of carriers. The current induced by this movement is then picked on electrodes, amplified and processed by some front end electronics.

The implementation of this concept varies greatly depending on the material from which the detector is constructed. In the following sections we will summarise the operational principles of silicon detectors

2.1   P-N Junction

Silicon is a semiconductor material. Its electrical properties can be modified by adding controlled impurities to the lattice; this process is called doping. There are two main types of dopants used: acceptor impurities and donor impurities (see Figure 2.1). Phosphorous is a typical donor dopant. It has 5 electrons in its outer shell. When added to the Si lattice, the extra electron is lightly bound. In the energy-momentum representation, the P atom introduces an energy level close to the conduction band. Phosphorous doped silicon is known as n-type silicon.
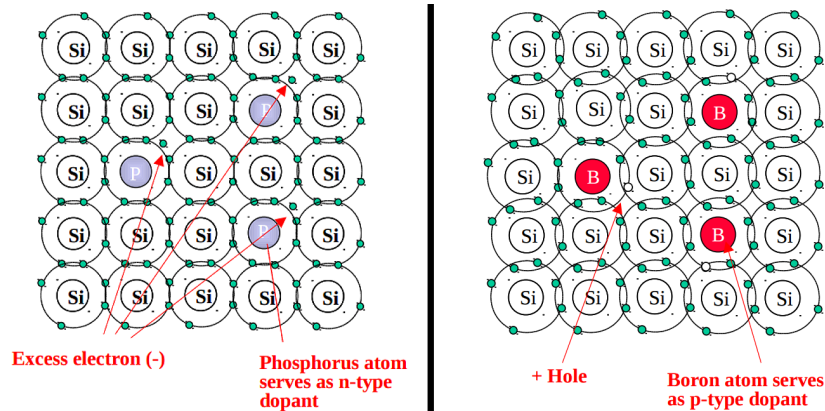
FIGURE 2.1: Sketch of doped silicon for both n (left) and p (right) doping types. For n-type doping Phosphorous is shown as example; Boron is used as example of p-type doping.

On the other hand, Boron is an example of acceptor dopant. Boron has 3 electrons in its outer shell. When Boron substitutes a Silicon atom in the lattice, an electron from a nearby Silicon atom will fill this deficiency. The Si atom contributing with the electron, will have a hole in its outer shell, that can be occupied with another electron from a neighbour atom. From a general perspective, the "hole" associated to the original Boron has now moved to another Silicon atom. This motion of a "hole" illustrates the conduction due to holes in a p-type doped Silicon.

These donor (or acceptor) levels introduced by impurities are very close to the conduction (valence) band. Energies of the order of $k_B T$ (with k_B being Boltzman's constant and T, temperature) at room temperature are enough to excite electrons (holes) from the dopant level into the conduction band (from the valence band into the impurity level). These addition of dopants to Silicon improves electrical conductivity of Silicon by orders of magnitude.

In a real semiconductor, there are impurities of both types, despite the fact that one kind of them can be majority. The difference between the number of donor impurities (N_D) and acceptor impurities (N_A) dictates whether the material is p-doped ($N_A > N_D$) or n-doped ($N_D > N_A$). This difference is called N_{eff}, or the effective doping concentration and is usually expressed in cm^{-3}

When n-type Silicon is put in contact with p-type a pn-junction is formed. Due to the concentration difference, electrons from the n-type will diffuse to the p-type material, while holes from the p-side will diffuse into the n-material. While doing so, an electric field appears from the n-type to the p-type material due to the fixed spatial charges (ionised atoms). This electric field will then stop diffusion of free carriers. The ionised atoms in the silicon lattice cannot effectively move from their initial positions.

The region depleted of lightly bound (free) charge carriers is called the depletion zone. Note that this region exists even in the absence of an external potential. The charge separation between the 2 oppositely doped volumes leads to an electrostatic potential. This voltage difference is called built-in voltage. If now a potential difference is applied such that the n- side is made positive with respect to the p-side, the depleted region will increase. This is called reverse biasing, and it is the electrostatic configuration needed to operate a detector.

2.1.1 Effective space charge distribution (Neff)

The electrical properties of the $p - n$ junction can be derived from Poisson equation.

$$\nabla^2 \phi = -\frac{\rho(z)}{\epsilon} \tag{2.1}$$

Where ϕ is the electrostatic potential, ϵ the absolute permittivity of silicon and $\rho(z)$ is the space charge distribution as a function of position (assuming here a 1D problem).

The value of N_{eff} therefore determines the potential and electric field in a non-irradiated detector. In the case of a simple p-n junction $\rho(z) = N_{eff}$ is a constant (the doping of the bulk). For now, we will focus on the non-irradiated case. We consider a junction located at $z = 0$, being $-z_p$ and z_n the extremes of the depleted zone in the p and n regions respectively.

It is important to note that since both the n-doped and p-doped silicon were electrically neutral at the beginning and no charge has been created or destroyed in the process of creating the junction, the material as a whole will remain neutral which means the total amount of charge has to be equal on both sides. This leads to a the mass action law, described as

$$N_A z_p = N_D z_n$$

For silicon particle detectors, one of the two sides is doped higher with respect to the other (e.g.: $N_A >> N_D$) and is deliberately thinner so that the depletion zone is almost entirely on one side of the junction ($z_n >> z_p$) as can be seen in Figure 2.2 a).
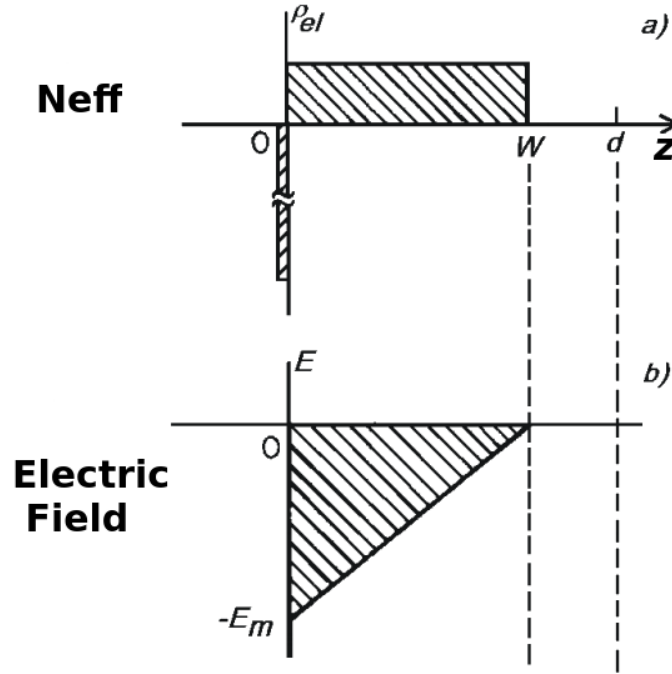
FIGURE 2.2: *a*) Sketch of the constant space charge distribution in a non-irradiated $p - on - n$ diode is presented here. *b*) The resulting electric field inside the diode is represented, the electric field is proportional to the depth z. The diode has a total thickness of d and it is depleted up to a depth w. In the Figure the junction is located at $z = 0$

With this configuration the width of the depleted zone (w) is $w \approx z_p$. When Poisson's equation is solved for $\rho = const$ the resulting electric $\nabla \phi = -\overrightarrow{E}$ field is linear with the distance to the junction interface(see Figure 2.2 *b*). In a typical detector configuration (where $w \approx d$) this means there is an electric field across the whole active volume of the detector (depleted area) in which any carrier created will move by drift.

2.2 Pad detectors

If the detector is partially depleted, then part of the detector will not be efficient to detect ionisation after a crossing particle. Indeed, the free charge carriers produced will recombine in the undepleted bulk. Therefore, the full detector needs to be depleted for optimal operation. For this purpose a bias voltage is applied following the same polarity as the built-in potential V_0 and increases the depleting effect of the $p - n$ junction therefore increasing the active volume of silicon.

Solving Poisson equation with bias voltage as boundary condition, the following expression is obtained:

$$w = \sqrt{\frac{2\epsilon V_{bias}}{\epsilon_0 N_D}} \tag{2.2}$$

What this equation shows is that the depleted volume ($w(V_{bias})$) increases as the square root of the bias voltage and that it decreases as the inverse of the square root of the doping of the bulk. Effectively, the higher the doping, the more difficult it is to deplete the device with a fixed voltage.
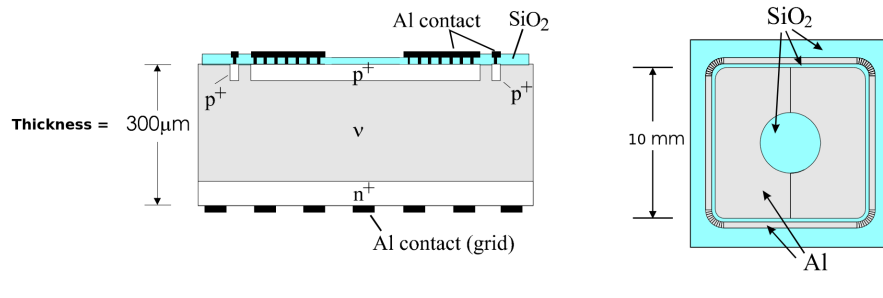

FIGURE 2.3: Sketch of a real silicon diode. On the left side a side view of the diode is presented and on the right side a top view of the diode is shown. The + superscript over p and n indicate heavily doped silicon while ν stands for lightly n-doped bulk.

The silicon pad detector remains one of the most important detector designs, particularly in research, due to its simplicity. Its design is presented in Figure 2.3 It is composed of a thin (typically 1μm) layer of very highly doped silicon, called the implant, that sits on top of a thicker (typically 300μm) piece of silicon with a lower volume density of dopants, called the bulk. Silicon particle detectors are bulk devices. Connection to the electrical circuit that provides the bias voltage and performs read-out of the signal is done by means of metal electrodes on the top part of the pad and an ohmic contact with a metal in the back.

2.3 Signal Generation: Ramo's Theorem

The depleted part of the silicon detector is the volume in which free charge carriers are created by ionisation and then drift inducing an electrical current in the electrodes. This instantaneous current can be time resolved and recorded for later analysis. This is the basis of the Transient Current Technique that will be explained in Chapter 4. The induced current in a system of electrodes can be readily calculated using Ramo-Shockely theorem[2].

The Ramo-Shockely Theorem states that the current induced by a moving charge in a system of electrodes is proportional to its charge, velocity and to a magnitude called

weighting field, that quantifies how the charge couples to an electrode. This weighting field is a purely geometrical factor. For instance, for a pad detector, the weighting field is a constant. In a microstrip detector the weighting field is very small when the charge is far from the electrode and is more important as it comes closer. Mathematically, the expression for the induced current is

$$i = q \cdot \overrightarrow{v} \cdot \overrightarrow{E_W} \tag{2.3}$$

where q is the elementary charge, $\overrightarrow{v}$ the drift velocity and $\overrightarrow{E}_W$ the weighting field. In 1D the vectors are replaced by their magnitudes.

For a system where more than one particle is moving and thus inducing current in the circuit, the total current can be written as the sum of each individual contribution (superposition theorem). If all the charge carriers have the same charge, as it is in the case for electrons and holes, drifting inside the silicon volume, then equation (2.3) can be re-written as:

$$I = q \cdot \sum_{n=1}^{N} \overrightarrow{v_n} \overrightarrow{E_W} \tag{2.4}$$

Note that though the charge for electrons and holes is opposite, they move as well in opposite directions and the currents from both add. The drift velocity is proportional to the electric field, the proportionality factor being the mobility. In silicon, mobility is only constant for low electric fields. Then it reduces as $1/E$. Like this, the drift velocity increases linearly with the field until a certain limit, where it reaches a plateau. The drift velocity thus saturates when the speed of the carriers equals the thermal speed of the electrons. Typically electron mobilities (μ_e) are taken to be referred to the conduction band unless otherwise specified. Conversely, hole mobilities (μ_h) are taken to be referred to the valence band by default. Putting all this together we arrive at

$$I = q \cdot \sum_{n=1}^{N} \mu_n(E) \overrightarrow{E} \cdot \overrightarrow{E_W} \tag{2.5}$$

Chapter 3

The effects of radiation in silicon detectors

When a particle goes through a silicon detector, it can loose energy via ionisation, which is a reversible process because the electrons extracted from the atoms will end up recombining in the material or going back to their original energy level via de-excitation. The impinging particle can also lose energy via non-ionising interactions, where the particle interacts with the Silicon atoms or with the dopant atoms. The effect is detrimental for the detector and leads to a reduction of the collected charge, amongst other macroscopical effects. It is important to understand these changes and have a parametrisation of the degradation. Understanding these defects is fundamental for designing radiation-hard detectors.

In this chapter we summarise the most important mechanisms of radiation damage. One of the key points of the project was to implement radiation damage on the TRACS simulator.

3.1   Damaging the lattice
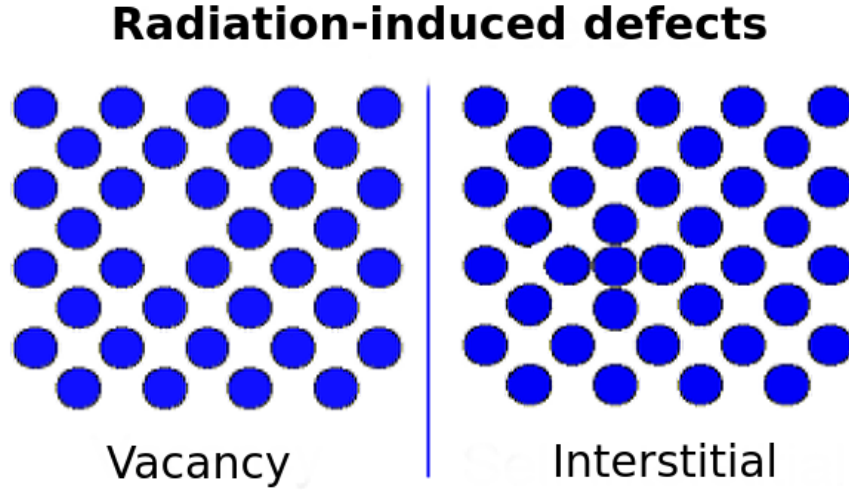
Radiation-induced defects

FIGURE 3.1: Interstitial (right) and Vacancy (left) lattice defects are illustrated here. These defects are be created inside silicon detectors after irradiation.

When a particle transversing the silicon bulk undergoes a non-ionising interaction one or more atoms get knocked-out from their equilibrium position in the lattice, disrupting the ordered structure of silicon. If the atom does not return to the equilibrium position, and Interstitial-Vacancy (I-V) defect is created. The term Interstitial refers to the knocked-off atom misplaced in the lattice and the Vacancy refers to the empty place that it leaves behind as shown in Figure 3.1. This type of defect alters the ordered structure of the lattice and creates a new energy level. The mechanisms by which the I-V defects degrade the performance of the detector and its practical consequences will be discussed in the next sections.

An impinging particle (or the recoil energy of the primarily knocked-off particle) can also create a cluster of defects. The size and clustering of the defects depends on the energy and type of radiation.

For example, according to [3], photons with up to 1 MeV energies will create only point defects and no clusters. Electrons can create both point defects and clusters, the latter only occurring for electron energies above 8 MeV. Neutrons will create mainly clusters starting at energies as low as 35keV.

Typically the NIEL (Non-Ionising Energy Loss) hypothesis is used to characterise the radiation damage caused by any type of particle. The NIEL hypothesis states that the damage produced by radiation of any kind of particle is proportional to the damage produced by 1 MeV neutrons. Therefore fluence of any type of radiation is rescaled to the equivalent fluence of 1MeV neutrons.

The I-V defects induced by radiation are not necessarily static defects and their size and configuration varies with temperature in time. For instance, the depletion voltage first decreases with time at a fixed temperature (so-called beneficial annealing) to increase linearly afterwards (long term annealing). Annealing depends heavily on temperature. Defect dynamics observed after 21h at 60C can be slowed down to about 500 years just by cooling down the irradiated detector to -10C [4]

3.2 Trapping effects

The defects induced by radiation affect the drift and collection of the $e - h$ pairs. The I-V defects can create so called $deep - levels$ that can trap and hold charge carriers for times longer than the typical collection times in silicon detectors. The result is a net loss in charge collection efficiency as well as a modified N_{eff} profile.
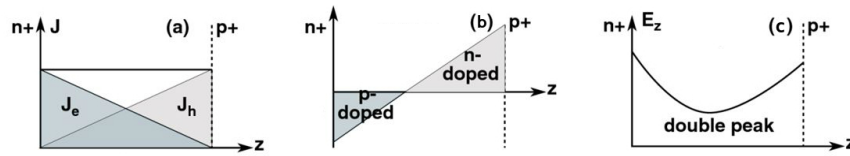

FIGURE 3.2: Explanation of the double peak origin is shown in this three schematic plots. *a*) The carrier current is shown for an diode as being proportional to depth. *b*) For evenly distributed trapping centres the number of trapped carriers is proportional to their current as shown in *a*). *c*) The electric field arising from carrier configuration shown in *b*) is plotted, the double peak feature becomes now apparent.

To explain why the N_{eff} gets modified after irradiation, we will follow the argument presented by V.Eremin[5]. The current density of e or h ($j_i(z)$), in a fully depleted silicon detector, is not a constant but has a linear dependence with thickness (z), as shown in figure 3.2*a*. The concentration of carriers ($n_i(z)$) is proportional to the current $j_i(z)$, so $n_i(z)$ is also linear with z. After enough radiation the defects and their correspondent deep levels can be considered uniformly distributed throughout the detector. Then more electrons will be trapped close to the n+ side, and more holes close to the p+ side, simply because the concentration of these carriers is higher there. As a consequence a net negative space charge appears near the n+ side and positive near the p+ side, leading to a N_{eff} profile linear in depth (see Figure 3.2*b*). For a more complete description of this argumentation and its validity the reader is referred to [5].

One of the consequences of having a non-constant N_{eff} configuration is that the resulting electric field inside the detector gets modified. In the linear case a parabolic electric field appears (see Figure 3.2*c*) giving rise to a characteristic *double peak* (DP) shape of the transient waveforms. Another consequence of not having a constant N_{eff} is the

appearance of a second $p - n$ junction at the end of the detector creating the double junction (DJ) effect. The existence of the DJ means that in a non-fully depleted detector both ends remain sensitive to radiation.

So far it has only been considered that the modification of the N_{eff} due to radiation-induced defects gives rise to a linear N_{eff} inside the detector. However, this might not be always the case, as it has been proposed in more recent publications[6]. Analysis performed using edge-TCT (see Chapter 4.2) techniques suggest that the N_{eff} configuration might have three different regions in which N_{eff} value is different. This parametrisation will be referred to as *triconstant* and can also explain the DJ and DP effects seen experimentally. As it will be explained in detail later, both linear and triconstant parametrisations have been implemented into TRACS as well as a third parametrisation consisting of three linear regions.

Besides altering the space charge profile, deep levels induced by radiation have also an impact on signal collected. When charge carriers drift through the irradiated volume they may get trapped in a radiation-induced defect and may remain there for as long as several miliseconds. This is much longer than the collection time of the electronics (of the order of tens of nanoseconds) so they are effectively lost for the electronics. As a result, the waveform shape gets distorted (as it will be explained in the following section) and the charge collected decreases worsening the performance of the detector.

3.3   Signal degradation

The effects of radiation in detector performance can be observed both in terms of the total collected charge and the shape of the transient waveforms. The modified N_{eff} distribution inside the detector has an effect on the shape of the waveforms while the effects of trapping centres can be seen both in the waveforms duration and amplitude and also in the total collected charge.

It has been explained in section 2.3 that the $I(t)$ profile of the collected signal from the detector depends on the $\overrightarrow{E}$ inside of it. It then follows that a modified N_{eff} (and consequently a modified $\overrightarrow{E}$) will have an effect in the collected signal and might show a double peak (DP) due to the previously mentioned DJ effect. The collection time might also be affected for the same reason.

For the trapping effects, the probability that a carrier drifting inside the silicon gets trapped in the radiation-induced deep levels after a time dt is

$$p_{trap} = 1/\lambda \cdot dt$$

with λ the effective carrier trapping distance that can be different for electrons and holes. We will use $\tau \approx \frac{\lambda}{v_{th}}$ with τ being the trapping time and v_{th} the thermal velocity of the carrier and can be used in most situations[7] since $v_{th} > v_{drift}$. τ is an experimentally determined parameter that is usually taken to be constant or dependant on the electric field and type of carrier. For the rest of the report we will consider τ to be a constant except otherwise stated. This allows to write the number of non trapped carriers N after drifting in the detector for a time Δt as [[7], pag 17]

$$N = N_0 \cdot \exp\left(\frac{-\Delta t}{\tau}\right)$$

where $N_0 = N(\Delta t = 0)$ the initial number of carriers generated in the detector. Since the intensity is the sum of every carrier's contribution, if we assume that every carrier contributes equally to the total current the previous equation can be re-written as

$$I(t) = I_0(t) \cdot \exp\left(\frac{-\Delta t}{\tau}\right) \tag{3.1}$$

where $I_0(t)$ is the current if there were no trapped carriers.

Chapter 4

Characterisation techniques (red and edge TCT)

Characterisation of detectors both before and after irradiation is of great importance to understand the effects of radiation and for trying to counteract them. Typical measurements performed include I/V and C/V characteristics as well as light illumination using Transient Current Techniques (TCT) in any of its variants.

The I/V and C/V are purely electrical measurements in which intensity (or capacitance) is recorded at different voltages. From the corresponding curves different detector parameters such as depletion voltage, breakdown voltage... can be calculated.

The most common optical techniques are TCT in which the silicon detector is illuminated using a laser. The resulting current generated due to the drift of charge carriers inside the detector is recorded over time. These *transient* currents or waveforms are later analysed and can provide information about many aspects of the detector.

In this work I/V and C/V measurements will not be considered in detail and focus will be placed on TCT measurements since these are the type of measurements that TRACS simulation software is able to reproduce. In the following sections we will explain the two main TCT techniques that are currently performed namely normal-TCT and edge-TCT. All of them share the same basic principles of illumination and signal recording.

4.1   Normal-TCT

In normal TCT, red or IR laser beams are directed to the front or back surface of the detector. Since silicon absorption coefficient depends on the wavelength of the light

it follows that different laser frequencies will have different penetration and will yield substantially different results. All these techniques exploit the fact that photons with enough energy can create electron-hole pairs that will drift inside the detector generating an electrical current.
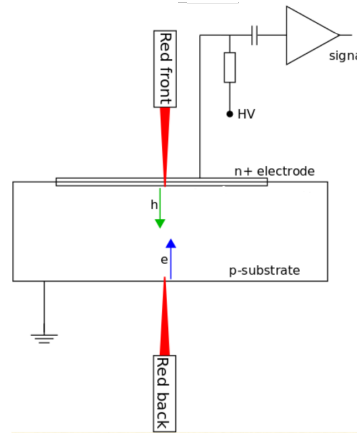

FIGURE 4.1: A schematic view of typical normal-TCT configuration using red laser is shown. In reality laser will illuminate the top or bottom of the detector but not both ends at the same time.

The most basic of TCT techniques is the so-called red-TCT. This kind of TCT measurements consist on illuminating the top or bottom part of the detector with a red laser with a typical wavelength around 660nm as shown in Figure 4.1. The absorption of these photons is a first order process since the energy of the incident photons is bigger than the minimum energy required to create an electron-hole pair. Silicon's absorption for red light is high and hence, all the photons are absorbed within a few μm from the edge.

All the electron-hole pairs are created in a small region very close to one of the collection electrodes. Taking top-TCT of a n-on-p diode as example, the laser is shot over the implant and barely reaches the bulk. After the charge carriers are created, the electrons are collected at the n+ implant in less than a nanosecond contributing to signal with just a very high and narrow spike in current, usually filtered by the bandwidth of the electronics (Bandwidth 2GHz). The holes, on the other hand, drift throughout the whole bulk of the detector leaving a much longer signal. When the laser is shot on the bottom of the detector the process is inverted with holes being quickly collected and electrons drifting through the whole detector leaving the longer signal imprint.

This type of measurement allows to obtain information about the electric field by simply using Equation (2.5). This information can be used to measure detector efficiency and also to compare silicon detectors before and after irradiation.

4.2 edge-TCT

To have a better control on carrier placement inside the detector, edge illumination can be employed. In edge-TCT measurements, the laser is shot from the side of the device (parallel to the implants and ohmic contacts) hence the '*edge*' naming convention. To increase the penetration depth of the light an infrared laser with wavelength around 1060nm is typically used. An schematic view of this configuration can be seen in Figure 4.2.
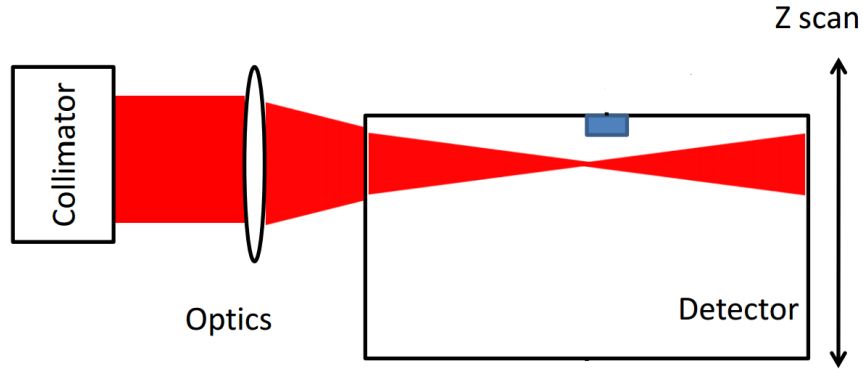

FIGURE 4.2: Schematic view of the edge-TCT configuration.

Typical edge-TCT scans are performed by sampling the whole detector height in steps and repeating this process for different bias voltage values.

One can also measure the width of the depleted area for a given voltage by performing an edge-TCT scan and measuring where the total collected charge starts to drop. The decrease in collected charge marks the transition between the drift region and the diffusion region where the detector is not depleted. The precision of this measurement is limited by the waist of the laser beam ($\sigma \approx 8 - 10\mu$ m). This limitation in precision and the lack of information in the direction of the laser beam are the only two limiting factors in edge-TCT measurements.

4.3 Experimental setup for (red) TCT measurement

The setup that will be described is specific for the TCT+ setup in the SSD[8] laboratory at CERN. However, most of the TCT capable setups share most features.

Only the setup for red-TCT measurements will be described since this is the kind of measurements to which TRACS simulations will be compared in Chapter 6. Other

TCT techniques are performed in similar manner with the main difference being the laser placement and movement.
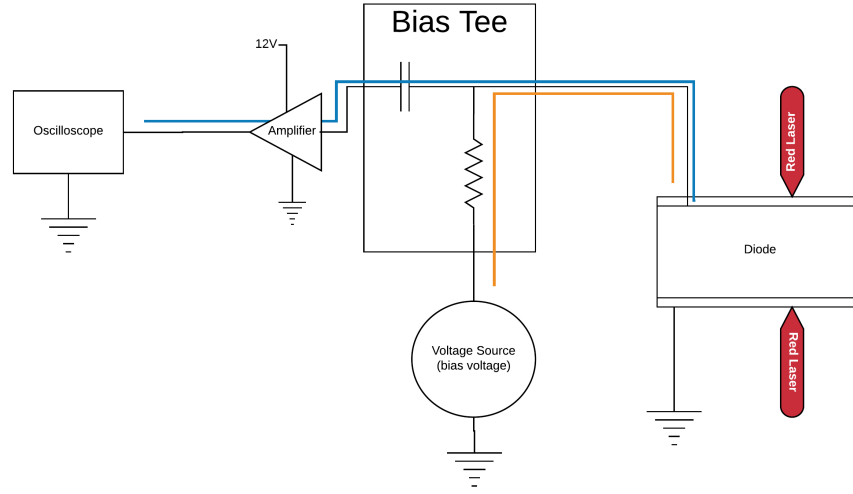

FIGURE 4.3: Simplified scheme of the circuit used in the TCT+ to perform red-TCT measurements. The separation of AC (blue line) and DC (orange line) components of the electrical signal is shown.

To perform TCT measurements there are some basic components that need to be present in the setup. These components and the connections between them are illustrated in Figure 4.3 with laser configuration in red-TCT position. The power supply provides the bias voltage for the operation of the silicon diode. Biasing and read out are done using the same cable. Therefore, the bias voltage from the power supply needs to be separated from the AC signal to the amplifier. This is crucial since most amplifiers can only take a few Volts as input while bias voltage is typically around hundreds of Volts and can surpass 1000V in some measurements. This AC-DC separation is achieved inside the Bias-Tee device thanks to the use of a Resistance-Capacitor as shown in Figure 4.3.

The transients (AC signal) from the detector get amplified and then reach the Oscilloscope, which in the case of TCT+ has a 50ps time resolution (20 GS/s[1]) and 2.5GHz bandwidth. The signal is recorded and processed; to reduce noise and signal fluctuations, the recorded transients are the average over several raw ones. Another common way to reduce noise is to use a Faraday cage to isolate the circuit from external interferences (e.g.: Wi-Fi, GSM...).

The Faraday cage is built in such a way that it also provides a dark environment to guarantee that charge generation inside the detector is only due to the laser illumination. The red laser used in TCT+ setup has a wavelength of 660nm and a pulse width of 300ps. The temperature is kept constant by using a Peltier device in contact with the diode;

---

[1]GigaSamples/second

this device also allows to remotely control the temperature of the diode during the measurements.

The whole setup is controlled via a custom LabView[9] program. The same software takes care of saving and storing the data on an ASCII file that is later analysed. The data analysis procedure is performed using software specially developed in the SSD group for this purpose and that can calculate and plot numerous physical parameters of interest such as charge collection efficiency, collection time. . .

Chapter 5

TRACS upgrade, description and implementation

According to speed and accuracy of simulation software, we could classify it in 2 categories: fast light-weight approximate simulators or slow, powerful, accurate simulators. The latter group being used for device design and performance prediction and the fast simulators commonly used for measurement comparison in laboratory situations.

Here we will focus on the fast and light-weight simulators since that is the software that was upgraded during this project.

In the silicon detector simulation field, specially amongst members of the RD-50 collaboration from CERN [10], there were several already available simulators capable of reproducing TCT measurements for different detector configurations (diode, micro-strips...) each of them (kDetSim, Weightfield2...) with some additional features. The software of choice for this project was the Transient Current Simulator (TRACS) developed by Pablo De Castro[1] in 2014 in the PH-DT-DD-SSD group at CERN.

The reason to use TRACS was based on two arguments. First one is that TRACS is an open-software platform built around efficient open-software libraries that have been exhaustively tested and validated by third parties. And second and probably more important is that the software TRACS was already developed and used in the PH-DT-DD-SSD group with future improvement in mind such as the one realised in this project.

In this chapter we will present the structural design of the software as it was before the project started including the different parts in which it is divided. This chapter

---

[1]Former Student of Universidad de Cantabria

is also intended to serve as additional documentation of TRACS. We will also present the changes and upgrades performed with particular emphasis on the implementation of radiation damage. Finally, we shall comment briefly on where the software stands now, after the upgrades, and what further improvements could be made.

5.1   Software design

TRACS is built and written in C++11 ISO standard [11] and makes use of Fenics [12] and Boost libraries [13] for calculations and Qt [14] and VTK [15] for GUI, plotting and visualisation. The whole software takes advantage of Object Oriented Programming and it is, thus, organised in different classes. TRACS also has two different operational modes available: a command line interface (CLI) and a Graphical User Interface (GUI) both of which will be explained in detail later in this section.

During a typical simulation of TRACS, the program takes detector properties (thickness, depletion voltage, geometry...) and carrier position (the laser is modelled by the charge deposition it produces). TRACS then solves Poisson's equation for the given conditions to obtain the electric field. This part is done using the aforementioned Fenics libraries taking advantage of their efficient PDE solver. Then the carriers are allowed to drift inside the detector using the electric field obtained in the previous step; Ramo's theorem is used to calculate the induced signal in the circuit. Waveforms are saved and stored in both plain text and ROOT[16] format. This process is shown in Figure 5.1 as a flow chart; some of the components of TRACS will be explained in detail in the following section.
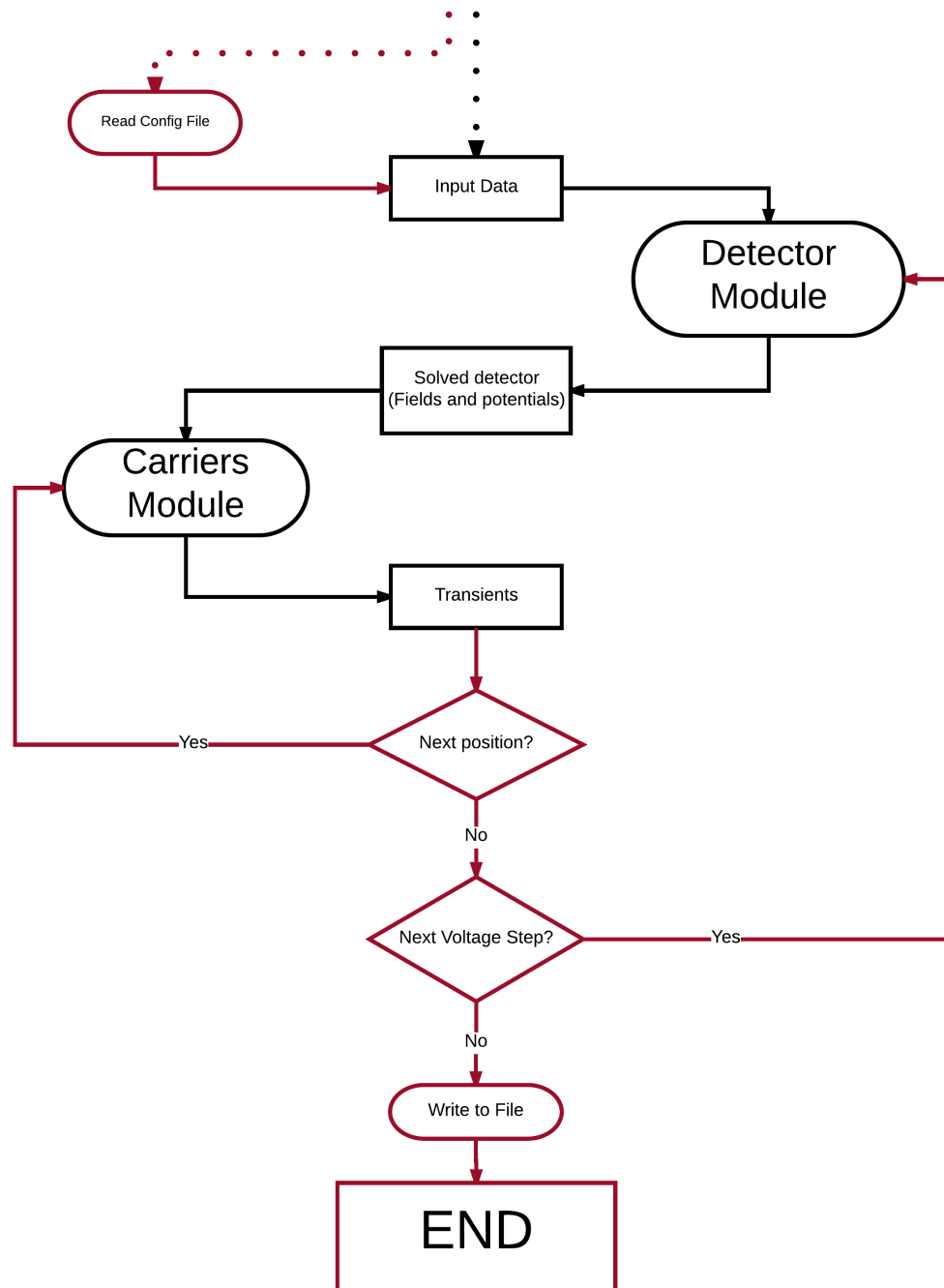
Run Software

FIGURE 5.1: Flow chart of the most general voltage and coordinate scan implemented in TRACS. It includes Command Line Interface only parts (dark red) and parts present in CLI and graphical mode as well (black). It is a simplified view of the simulation process. Rounded shapes represent processes and rectangles represent the intermediate results.

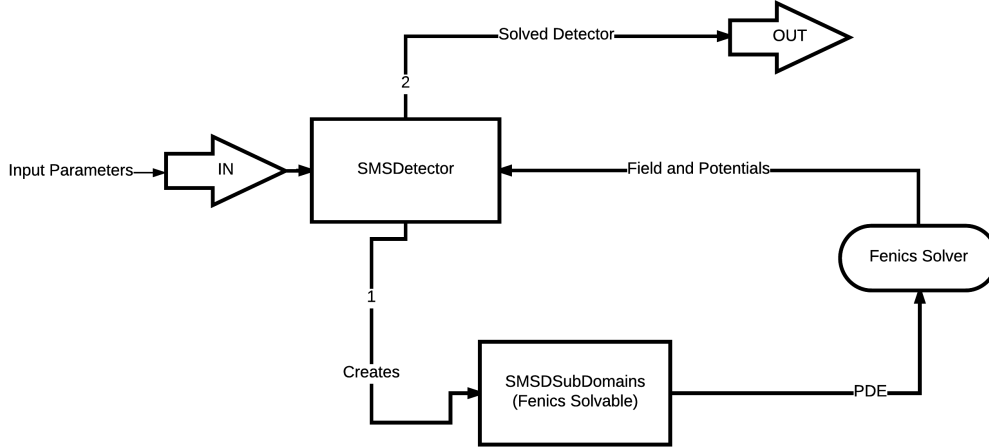### 5.1.1 Detector module and Partial Differential Equations solver

FIGURE 5.2: Flow chart of the behaviour of the so-called Detector Module. This is a simplified representation of the process by which the detector is initialised and the fields and potentials inside are calculated.

One of the core modules of TRACS is that composed of the detector class and PDE solver which has been called "Detector Module"; its behaviour is depicted in Figure 5.2. The main classes of the module are *SMSDetector* and *SMSDSubDomains*. In the first, detector properties (geometry, electric field inside...) are stored as attributes that allow the class to represent a detector. The class *SMSSubDomains* serves as a bridge between the *SMSDetector* class and Fenics solver; geometry and boundary conditions are stored inside of it in such a way that Fenics solver is capable of understanding and solving the PDE.

The PDE solving algorithm is fully provided by Fenics libraries and the configuration done through *Poisson.h* and *Gradient.h* files. The electric and weighting potentials and fields obtained after solving Poisson's equation are stored in the class *SMSDetector* as attributes of Fenic's internal type *Function* and are accessible through public *getter* methods.

If several simulations are to be performed using the same detector and initial conditions, the fields and potentials need not be calculated since they are saved in memory by TRACS.

This part of the software is flexible enough to accommodate for any detector geometry with few changes in the code, thanks to the use of Fenics. Diodes and micro-strips are simulated out-of-the-box. In particular, diodes are considered a special case of micro-strips with just one strip covering the entire surface of the detector.

It is in this part of the software that N_{eff} is calculated through the value of V_{dep} for the non-irradiated case, see equation 2.2. Several modifications were done in TRACS to extend its capabilities of simulation to a radiation-modified N_{eff} parametrisation decided by the user. We will explain the modifications in the next section as we go through the modifications performed to TRACS.

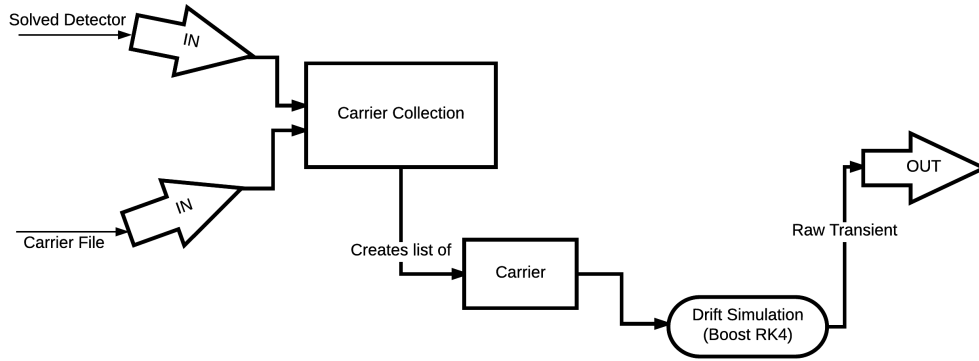### 5.1.2   Carriers Module and drifting

FIGURE 5.3: Flow chart of the behaviour of the Carriers Module is presented. This is a simplified view and doesn't show all the classes present in the module as it is intended only to represent the behaviour of the module.

After the electric and weighting fields and potentials have been calculated, the software proceeds to move the charge carriers inside the detector. This is handled by the classes: *CarrierCollection, Carrier, CarrierMobility, CarrierTransport*. A flow chart of the behaviour of this module can be seen in Figure 5.3.

The charge carriers are input via an ASCII file automatically produced for the user using python scripts. The scripts are not distributed with TRACS but carriers files can be created by users following the current format. The carriers file contains one carrier per line with initial position (in the 2-D section of the detector), the off-set time at which they should be generated in the simulation, and the equivalent charge they carry. The carriers can be moved about the detector if needed so that the user does not need to simulate the movement of the laser. The current is calculated using Ramo's theorem for every carrier and added together for every time step.

A time offset in the input file is used to shift the start position of the waveform. This is useful to match the measured and simulated waveforms.

Simulating the movement of carriers inside the detector requires to solve the first order differential equation[17]

$$\frac{d\vec{x}(t)}{dt} = \vec{v}(t) = \mu \vec{E}(\vec{x}(t))$$

That is taken care by Runge-Kutta-4 method implemented inside ODEINT libraries. ODEINT libraries now come as a standard part of BOOST libraries inside C++11. These libraries, together with Fenics, ensure fast, efficient and robust computational properties at the core algorithms.

5.1.3   Joining all together (CLI and GUI)

To bring all the components together TRACS has both a CLI and a GUI available to the user. TRACS is designed around two main use case scenarios: quick checks and long simulations. For the latter case CLI was designed, providing the user with an easy, low resource execution version, that can be easily automated.

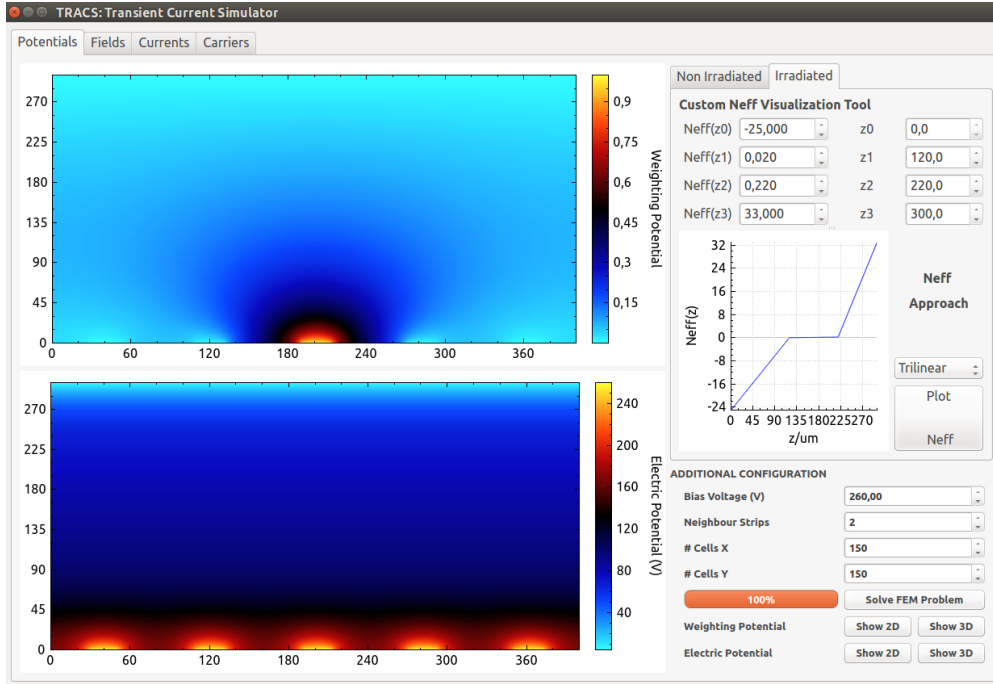### 5.1.4   GUI and its advantages

FIGURE 5.4: Screen-capture of TRACS' GUI. The GUI provides 4 different tabs that allow for easy and fast simulation of various scenarios including single particle, line of carriers and custom carrier distribution. The tab shown here shows the interface for parameter input and detector solving.

Besides the already mentioned CLI, TRACS also provides a GUI (see Figure 5.4) to allow for easy checks and a more user-friendly approach to simulations. It is divided in different tabs for each of the different components of TRACS.

First tab allows the user to configure all the detector parameters and solve the PDEs for the specific detector parameters. After resolution of the PDEs, all the potentials and

fields are plotted inside the potentials tab and the fields tab respectively. The graphs offer colour-coded 2D maps as well as 1D cut of the fields; interactive 3D plots are also available through VTK tools.

The other two tabs are used for carrier drifting and waveform simulation. Options range from 1 carrier simulations and simulation of a line of carriers to full laser illumination simulations (provided that an externally generated file is present). The Carrier tab is equipped with a carrier visualisation window (to display the carrier generation shape) and a waveform visualisation window (to study the simulated induced current). TRACS-GUI also allows saving the waveforms in plain text format.

5.1.5 Approximations and limits of TRACS

TRACS needs to make some approximations to reduce the computational requirements of the simulations. A rough 10% precision loss can be estimated from these approximations, when compared to real data.

TRACS solves internally the necessary PDEs in 2D only because a planar detector can be approximated as being a 2D structure. However, because TRACS makes use of Fenics libraries it is possible to implement 3D detectors in the future if required.

Another approximation made by TRACS is neglecting any electron-electron (or hole-hole) interactions inside the detector. It is a justified since the $\overrightarrow{E}$ inside the detector are many orders of magnitude greater than the $\overrightarrow{E}$ due to all the carriers.

An important feature of the TRACS carriers simulation is the grouping and splitting of carriers by assignment of a weighted charge. This means that groups of charge carriers of the same type, lying initially very close together, can be simulated as being just one charge carrier with a total charge equal to the sum of all the individual charges of the carriers. This reduces greatly the number of individual charge carriers that need to be simulated hence improving simulation times. This grouping can be done with almost no penalty in precision of the results as carrier-carrier interactions are neglected.

The thermal diffusion of charge carriers inside the detector is also neglected in TRACS. The thermal diffusion is mostly important in the undepleted bulk. In the depleted zone it adds a smearing of few microns to the final position of the carriers. A consequence of this simplification is that TRACS is only accurate when simulating fully depleted detectors.

5.2   TRACS upgrade

All the modules and features we have explained in the previous section were part of the original TRACS software. From that point the software was modified and upgraded to *1)* include radiation damage effects with user defined parameters and *2)* improve the usage of TRACS both as a standalone and as a library-like module for bigger projects.

5.2.1   Modifications to TRACS

The different effects of radiation damage in the signal obtained from a silicon detector have been discussed before and we concluded that besides the change in V_{dep} and leakage current, the main effects were the loss in charge collection efficiency and the modification in the shape of the waveform due to the perturbated N_{eff} . These effects are all the result of the Vacancy-Interstitial defects in the lattice due to particle-Si collisions.

In TRACS three models for the change of N_{eff} with fluence were included.The first one, the linear approximation, has only 2 free parameters that would need adjusting. This parametrisation has given good results in modelling N_{eff} modification in irradiated silicon detectors.

The second modelling of the N_{eff} (already introduced in section 3.2) consists on 3 different areas where the carrier density is constant. The third model is a combination of the two previous models. The N_{eff} configuration is assumed to have three different zones in which it is linear with depth.

In the linear approximation, continuity and derivability are guaranteed as it consists of only one straight line. Derivability, though not strictly necessary for current use of TRACS, has been ensured in both triple linear and triple constant approximations by means of hyperbolic tangents connecting the end of one area with the beginning of the adjacent one. Continuity in the triple constant approximation arises from these hyperbolic tangent bridges that connect smoothly one value of the N_{eff} in one area to the vale in the next; in the triplelinear case continuity is forced because the parametrisation requires that adjacent N_{eff} zones have the same value at the interface point.

Trapping of charge carriers is a statistical process and it would require for each carrier, a probability evaluation after each step with the corresponding performance penalty, specially for low trapping probabilities and high number of carriers.

To avoid such computational overhead, we opted for the approximated implementation of the effect through the use of an exponential wrapping over the whole waveform. The physical justification of the approximation has already been explained in section 3.3.

This approximation requires enough simulated time and enough carriers to be accurate enough.

The last of the upgrades to TRACS was the inclusion of electronics shaping. TRACS had lowpass filter shaping as an option in CLI version but that was not good enough for detailed comparisons to measured data. We implemented electronics shaping by convoluting the raw signal (or the low pass filtered one) with the amplifier transfer function.

Another important change to the CLI was the addition of a configuration file was added to the code, together with the necessary *parser*, eliminating the need for recompilation every time an input value is changed, and making it possible for users to change simulation parameters in CLI without the need to dig into the code. The code (existing and new) was also commented and documented.

TRACS execution options were expanded with the inclusion of the new class *TRACSInterface* that allows the simulation to be called as a a library from an external user code.

The *TRACSInterface* class contains a simple set of methods that allows the user to read the input values from the configuration file, modify those parameters and perform every step of the whole simulation as well as returning results. The creation of this library avoids compilation of TRACS sources every time the user code is to changed.

5.2.2   Implementation of TRACS upgrade

Implementation of the improvements in TRACS did not present any significant design problems due to the usage of Object Oriented programming and external flexible libraries. In the case of modified N_{eff} implementation Fenics libraries provide users with the option to define a custom space charge distribution to solve Poisson's equation.

By creating a new class *Source* the N_{eff} could be parametrised. Inside the class, *Setter* methods were also implemented so that N_{eff} approximation and parametrisation can be modified at run-time. By having a dedicated class for N_{eff} parametrisation TRACS can also be easily extended to account for any other new parametrisations.

For both N_{eff} parametrisation and trapping effects, it is needed for the user to input the relevant parameters. For the custom N_{eff} effect the input data are the coordinates of the points needed to define the selected N_{eff} parametrisation. The number of parameters needed in each case varies from 2 for the linear case to 5 for the triple constant N_{eff} to 6 for the case of triple linear approximation. In the case of trapping effects, only one parameter is needed: τ.

The configuration file, *Config.TRACS*, was added with its own syntax that allows the parser to distinguish input values from comments.

The GUI version of TRACS has also been upgraded to account and make use of the changes for simulating irradiated detectors. These changes include the extra fields to input the new parameters such as N_{eff} parametrisation type and coordinates, trapping time and a toggle to switch between simulation of irradiated detectors or non-irradiated detectors.

Other improvements to TRACS-GUI include the implementation of RC shapping capabilites for output waveforms as well as resizable plots throughout all tabs. The last of the visual improvements to TRACS is the inclussion of the Custom N_{eff} Visualization Tool which allows the user to preview the N_{eff} profile before starting the simulation.

5.3   Summary

TRACS has been improved and upgraded to include radiation effects into the simulations with user defined N_{eff} and trapping parameters. On top of those improvements TRACS, documentation was also extended. Flexibility was added so that now TRACS can run as an additional library in an external user code.

The original version of TRACS showed excellent agreement with experimental data from laboratory measurements[18] so it is expected that the new version of TRACS be a useful and accurate tool. This accuracy will be tested in the next section.

Chapter 6

Validation of TRACS for irradiated silicon detectors

A first way to attest the validity of TRACS results after the implementation of radiation damage is to compare simulation results to other measurements already published. In [19] it is shown how a linear parametrisation of the N_{eff} can be used to reproduce measurements of irradiated sensors accurately.

In a second step, TRACS simulation will be compared to our own measurements using the experimental setup described in Chapter 4.

TRACS is able to reproduce any kind of TCT measurement provided the carrier distribution inside the detector is given. The choice was made to perform red-TCT measurements in the TCT+ setup at CERN-SSD[8]. In particular bottom-TCT was chosen after several measurements since it best shows the Double Peak structure explained in section 3.3.

As already explained in the former chapter, TRACS needs between 3 and 7 parameters to model radiation damage (N_{eff} unknowns and trapping). To obtain the best parameters that describe the data we have followed a trial/error approach. Evidently, this is a solution chosen to show the validity of the simulation and can not be considered as a general solution. Indeed, the road-map of TRACS upgrades is led by an automatic fitting program that would extract the right parameters comparing data with simulated currents.

The parametrisation obtained will be considered as an effective parameter set that describes the data. The simulation-measurement comparison will only attest TRACS validity but not TRACS accuracy.

The detector used was a diode previously irradiated to $10^{15} n_{eq}/cm^{-2}$. It is a 300 μm thick diode with an active area of 1×1 cm^2 with a structure similar to that explained in section 2.2.

6.1   Experimental procedure

For the first comparison, the published measurements [19] were digitalised using an online tool [20]. Then simulations were performed using TRACS with the same input parameters as in the reference. Comparison of both sets of transients is presented.

For the second comparison (to measured data) we used a red-TCT configuration of the TCT+ setup described in Section 4.3. The laser was shot at the backside of the detector and a voltage scan was performed recording the transients generated with bias voltage ranging from 0V to 140V in steps of 10V. The measurements were performed with the detector at fixed temperature T = 273K

The data will be normalised to the maximum value of the histograms. In this way the direct comparison will be easier and the intensities of the laser will be factored out.

6.2   Comparison between TRACS and published data

To compare TRACS to published data, measurements from [19] will be used. In [19], N_{eff} is parametrised as a linear function of depth; the same parametrisation was used here. Since the raw data is not published, it was needed to digitise the plots published in the reference.

The transients from the reference are compared with TRACS simulations in Figure 6.1. Trapping simulation is different between both simulators, with TRACS having a constant τ while the reference uses a field-dependant τ.
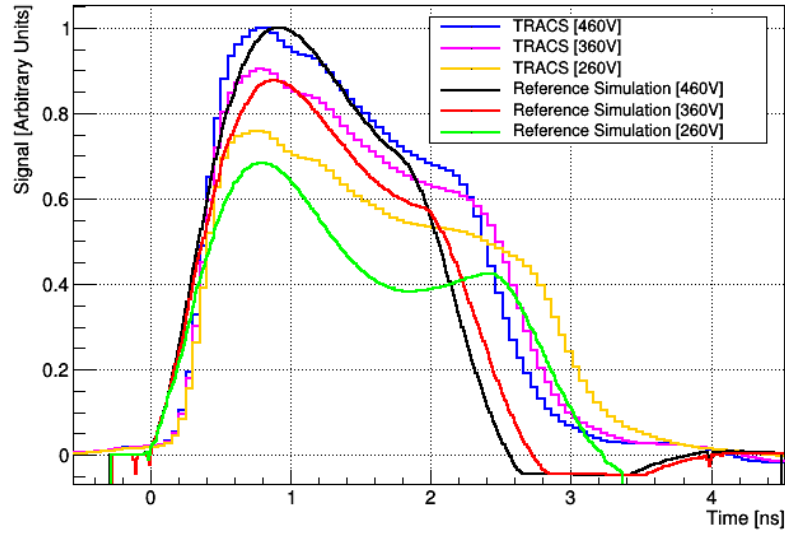
FIGURE 6.1: Transient currents generated by top-TCT measurements (continuous line) and simulations(histogram). TRACS uses a different trapping parametrisation yielding different results while maintaining the general features of the measurements from [19]

6.2.1 Comparison between simulations and measurements

In order to reproduce the transients obtained using the TCT+ setup a trial/error method was performed manually. Trapping constant was chosen to be: $\tau = 4ns$. The chosen N_{eff} parametrisation was the Trilinear form. A plot with the 8 defining values for the chosen N_{eff} is presented in Figure 6.2.
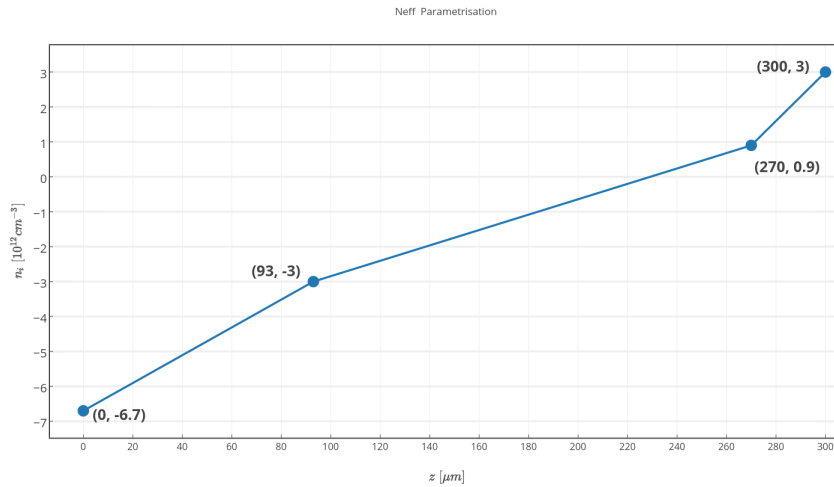

FIGURE 6.2: Representation of the N_{eff} parametrisation used for TRACS simulations. The Trilinear parametrisation was used and the values of the defining parameters are shown.

The data measured by the author is presented now. In the following plot all the transients measured in the laboratory are presented together. As it can be seen in Figure 6.3, the Double Peak feature appears only for bias voltage $\geq 80V$; this value of bias voltage can be considered a good estimation of the V_{dep}. The transients get shorter in time with increasing voltages and the second peak getting higher with increasing voltages.
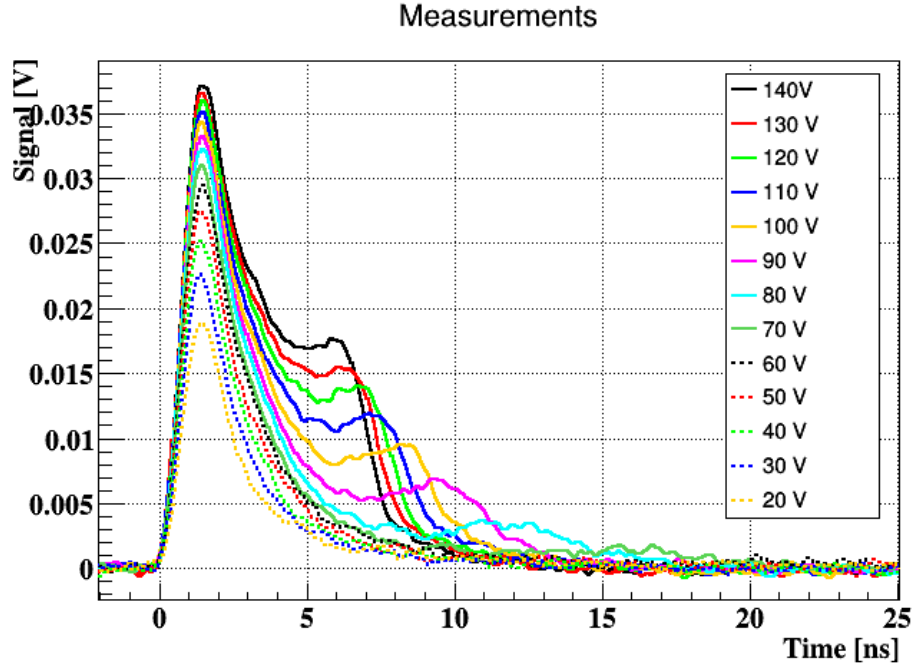

FIGURE 6.3: Measurements performed in the SSD facilities. The irradiated diode presents signs of radiation damage (DP). This transients serve as reference to compare with TRACS simulations

TRACS simulations are presented in Figure 6.4 in the same way as the measurements. It can be seen that TRACS simulations follow a similar trend of shorter transients and higher second peaks with increasing voltages.
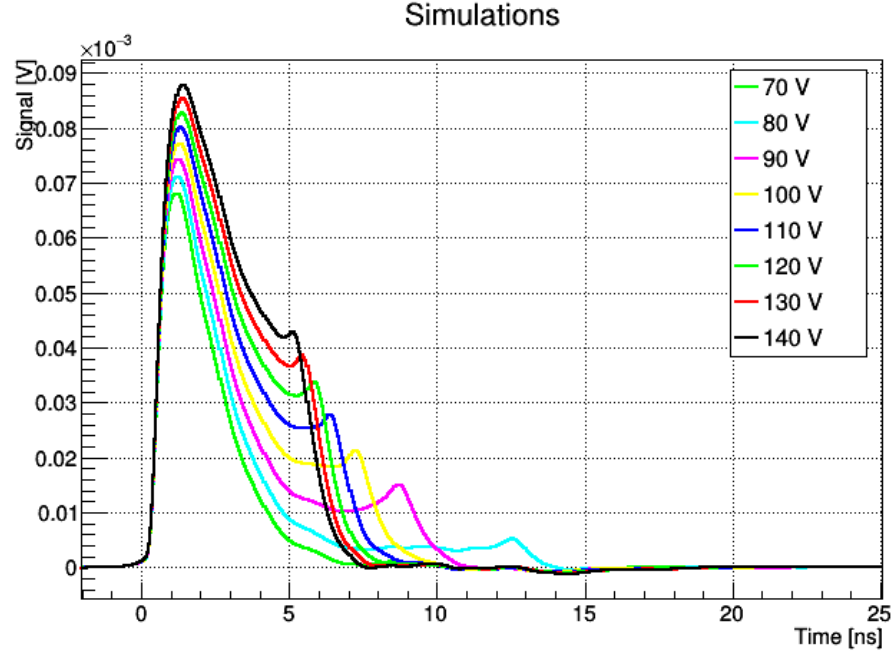
FIGURE 6.4: Simulations performed by TRACS. The triple linear approximation was used for the simulation. The simulated transients present similar features as the measured data.

No transients below $80V \approx V_{dep}$ were not simulated because TRACS does not simulate underdepleted detectors. For voltages bellow 80 V, the depleted region does not reach the backside of the detector, and the carriers created by the red laser are therefore not able to reach the drift region. The only chance for them to make it would be via diffusion, but TRACS currently does not simulate carrier diffusion. That is the reason why the simulation starts at 80 V.

From the previous voltage scans, three transients were selected, namely: 80V (Figure 6.5), 100V (Figure 6.6) and 140V (Figure 6.7).
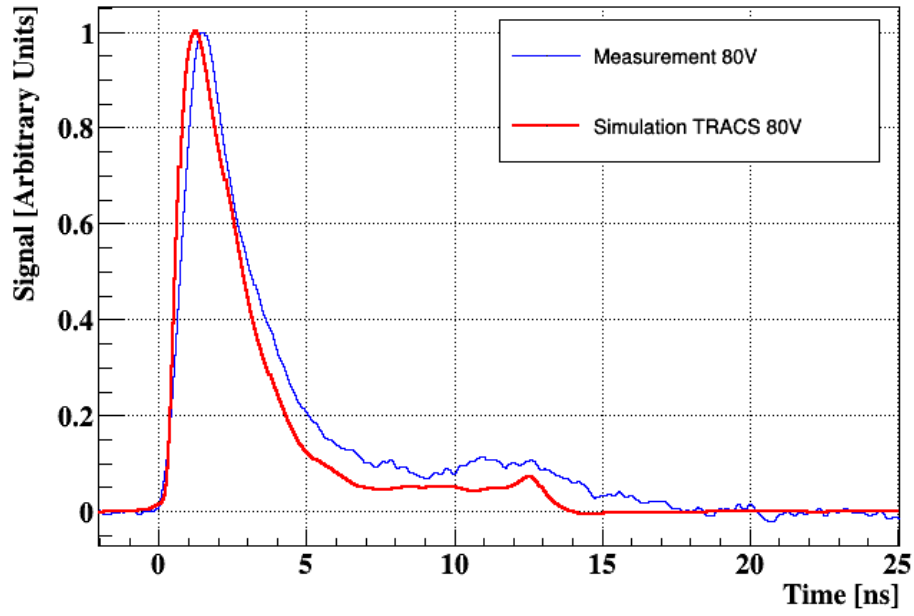
FIGURE 6.5: Comparison of the measured transients (blue line) and the simulations from TRACS (red line) for a bias voltage $V = 80V$.
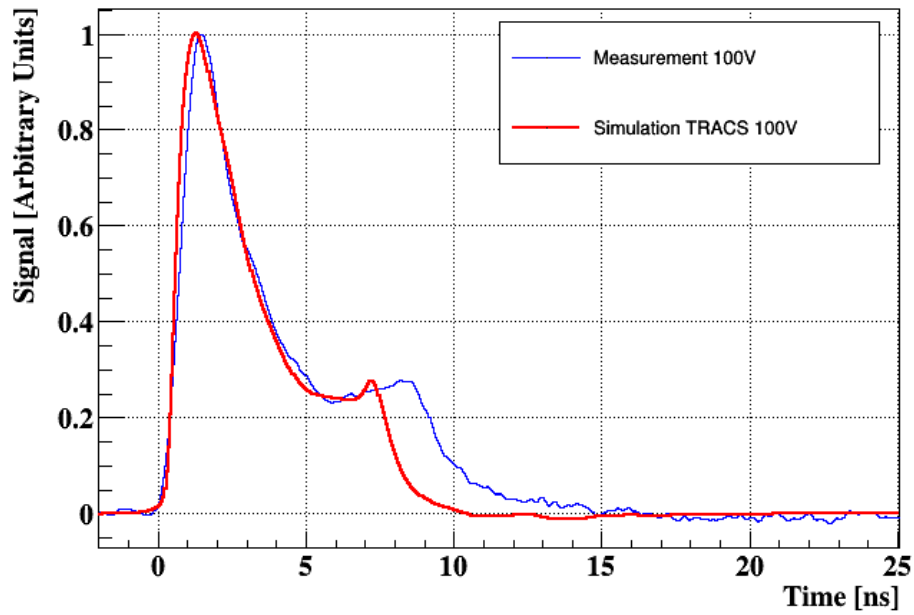

FIGURE 6.6: Comparison of the measured transients (blue line) and the simulations from TRACS (red line) for a bias voltage $V = 100V$.
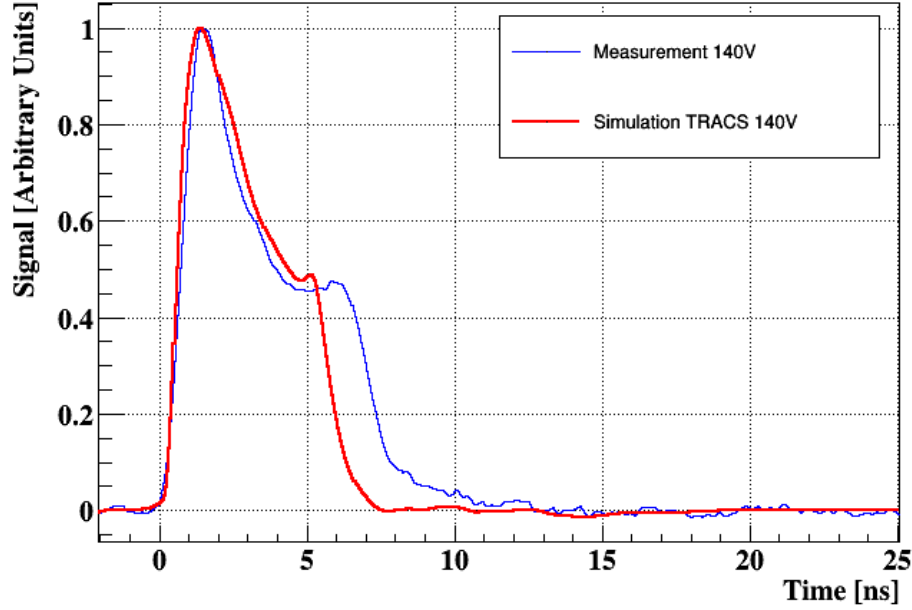
FIGURE 6.7: Comparison of the measured transients (blue line) and the simulations from TRACS (red line) for a bias voltage $V = 140V$.

Comparison of waveforms from Figs 6.5-6.7 shows that TRACS simulations exhibit similar features and behaviour as the measurements. Transients tend to be higher than measurements for higher bias voltage and lower than in the measurements for lower bias voltage ; a field-dependant τ could solve this discrepancy. The best agreement is found for high field and, thus, high current situations ($t < 5ns$) where diffusion has a smaller impact on the total current.

The fact that the simulations do not match perfectly the measurements can be attributed to the absence of diffusion in the simulation, the unknown space charge profile parameters (and real shape), the usage of a constant trapping time and the approximate electronics shaping used in the simulation.

6.3 Conclusion

Simulation data from TRACS has been compared to published measurements as well as compared to measurements performed by the author. In both cases TRACS transients exhibit similar features to those present in the measurements. Taking into account that an error of about 10% in TRACS transients can be attributed to approximations and that the method available for optimising the simulation parameters (trial/error method) is not optimal, it can be said that simulations and measurements from TCT+ setup are

compatible since they differ about 10% or less. It is therefore shown that TRACS can reproduce TCT measurements on irradiated silicon detectors.

Chapter 7

Conclusions and further development

The open software application TRACS has been upgraded so that is capable of simulating the transient currents of an irradiated silicon detector. To reproduce the radiation damage in these devices trapping effects as well as three different N_{eff} parametrisations (Linear, Triple Constant and Triple Linear) are available to the user.

Simulations have been timed to take $\sim 30s$ per transient simulated with reasonable simulation values. Simulations performed with TRACS have been compared to measurements and it was found agreement between both. The agreement proves that TRACS can be used as a tool to estimate the N_{eff} inside a silicon detector which was the ultimate goal of this project.

TRACS has also been improved with better documentation and with the inclusion of TRACSInterface. This new feature allows for TRACS to be used as a library by a external software. All these improvements together make of TRACS a fast simulator capable of reproducing the effects of radiation in the transient currents of silicon detectors. Future improvements include the integration of TRACS within a fitting software that can obtain the N_{eff} distribution of a silicon detector given the transients produced in the lab. For that purpose performance needs to be improved by means of parallelisation.

Bibliography

[1] Marcos Fernández Pablo de Castro, Álvaro Díez. Transient current simulator, 2014. URL https://github.com/IFCA-HEP/TRACS.

[2] S. Ramo. Currents induced by electron motion. *Proceedings of the IRE*, 27(9): 584–585, Sept 1939. ISSN 0096-8390. doi: 10.1109/JRPROC.1939.228757.

[3] Alison G. Bates and Michael Moll. Characterization of silicon sensors after irradiation with fast particles, July 2005. URL http://slideplayer.com/slide/8144849/.

[4] Michael Moll. *Radiation damage in silicon particle detectors: Microscopic defects and macroscopic properties*. PhD thesis, Hamburg U., 1999. URL http://www-library.desy.de/cgi-bin/showprep.pl?desy-thesis99-040.

[5] V. Eremin, E. Verbitskaya, and Z. Li. The origin of double peak electric field distribution in heavily irradiated silicon detectors. *Nucl. Instrum. Meth.*, A476: 556–564, 2002. doi: 10.1016/S0168-9002(01)01642-4.

[6] Gregor Kramberger, V. Cindro, I. Mandic, M. Mikuz, M. Milovanovic, and M. Zavrtanik. Electric field modeling in heavily irradiated silicon detectors based on Edge-TCT measurements. *PoS*, Vertex2012:022, 2013.

[7] Gregor Kramberger, Vladimir Cindro, and Marko Mikuz. *Signal development in irradiated silicon detectors*. PhD thesis, Ljubljana U., Ljubljana, 2001. URL http://cds.cern.ch/record/1390490. Presented 21 Jun 2001.

[8] Solid State Detectors group. Ep-dt-dd-ssd (cern semiconductor laboratory). URL http://ssd-rd.web.cern.ch/ssd-rd/default.htm.

[9] Chance Elliott, Vipin Vijayakumar, Wesley Zink, and Richard Hansen. National instruments labview: A programming environment for laboratory automation and measurement. *JALA: Journal of the Association for Laboratory Automation*, 12(1): 17–24, 2007. doi: 10.1016/j.jala.2006.07.012. URL http://dx.doi.org/10.1016/j.jala.2006.07.012.

[10] R&D Collaboration (RD50). Radiation hard semiconductor devices for very high luminosity colliders. URL http://rd50.web.cern.ch/rd50/.

[11] ISO/IEC. Iso international standard iso/iec 14882:2014(e) – programming language c++ [working draft], 2014. URL Retrievedfromhttps://isocpp.org/std/the-standard.

[12] Martin S. Alnæs, Jan Blechta, Johan Hake, August Johansson, Benjamin Kehlet, Anders Logg, Chris Richardson, Johannes Ring, Marie E. Rognes, and Garth N. Wells. The fenics project version 1.5. *Archive ootNumerical Software*, 3(100), 2015. doi: 10.11588/ans.2015.100.20553.

[13] Boris Schling. The boost c++ libraries, 2011.

[14] Qt Company Ltd. Qt — cross-platform software development for embedded & desktop. https://www.qt.io/, 1994–Current.

[15] William J. Schroeder, Lisa Sobierajski Avila, and William Hoffman. Visualizing with vtk: A tutorial. *IEEE Computer Graphics and Applications*, 20(5): 20–27, 2000. URL http://dblp.uni-trier.de/db/journals/cga/cga20.html#SchroederAH00.

[16] R. Brun and F. Rademakers. Root - an object oriented data analysis framework. *Nucl. Inst. & Meth. in Phys. Res. A 389 (1997) 81-86*, September 1996. URL http://root.cern.ch.

[17] Pablo De Castro Manzano. Simulation of drift dynamics of arbitrary carrier distributions in complex semiconductor detectors. *CERN CDS*, Sep 2014. URL https://cds.cern.ch/record/1755231.

[18] Marcos Fernandez Rogelio Palomo Michael Moll Pablo de Castro, Ivan Vila. Tracs : Transient current simulator, November 2014. URL https://indico.cern.ch/event/334251/contributions/780740/attachments/652578/897322/RD50_TRACS_20_11_2014.pdf.

[19] Thomas Pohlsen. *Charge collection and space charge distribution in neutron-irradiated epitaxial silicon detectors*. PhD thesis, Hamburg U., 2010. URL http://inspirehep.net/record/855436/files/desy-thesis-10-013.pdf.

[20] Ankit Rohatgi. Webplotdigitizer, May 2016. URL http://arohatgi.info/WebPlotDigitizer.